

Synthesis and structural investigations of bulky imino- and amido-phosphine palladium dimers

Sofia I. Pascu ^{*,1}, Grant D.W. Anderson, Malcolm L.H. Green ^{*}, Jennifer C. Green ^{*},
Nicholas H. Rees ¹, Andrew R. Cowley ¹

Inorganic Chemistry Laboratory, University of Oxford, South Parks Road, Oxford OX1 3QR, UK

Received 4 November 2005; received in revised form 14 December 2005; accepted 18 December 2005

Available online 17 February 2006

This paper is dedicated to Professor D. Michael P. Mingos on the occasion of his birthday.

Abstract

The reactions of palladium(II) dimers $[\text{Pd}_2\text{Br}_2(\text{L}1)_2]$ and $[\text{Pd}_2\text{Br}_2(\text{L}2)_2]$ (where $\text{L}1^-$ is $[\text{Ph}_2\text{PCH}=\text{C}(\text{Ph})\text{N}(2,6\text{-}i\text{Pr}_2\text{C}_6\text{H}_3)]^-$ and $\text{L}2^-$ is $[\text{Ph}_2\text{PCH}=\text{C}(\text{Ph})\text{N}(2,6\text{-Me}_2\text{C}_6\text{H}_3)]^-$) with AgBF_4 in a mixture of CH_2Cl_2 and MeOH give palladium(I) dimers $[\text{Pd}_2(\text{HL}1)_2][\text{BF}_4]_2$ and $[\text{Pd}_2(\text{HL}2)_2][\text{BF}_4]_2$, respectively. These exhibit unusual coordination geometries of the metal centre. Density functional theory (DFT) calculations showed that a phenyl ring of the bridging phosphine is involved in bonding via a delocalised metal-phosphine–phenyl interaction. The remarkable kinetic stability of these palladium(I) species may explain the early termination steps in the CO/ethylene copolymerisation reaction catalysed by Pd(II)–amidophosphines or enolisable Pd(II)–iminophosphines.

© 2006 Elsevier B.V. All rights reserved.

Keywords: Pd(II) dimers; Pd(I) dimers; Amidophosphines; Iminophosphines; CO ethylene copolymerisation; Density functional theory

1. Introduction

There is considerable industrial and academic interest in palladium(II) chemistry and its involvement in homogeneous catalysis of C–C coupling reactions. Coordination chemistry of hybrid P/N ligands has been the focus of attention due to their mixed hard–soft character and potentially hemilabile behaviour. The use of palladium(I) dinuclear species as catalysts has emerged recently [1–9] especially in cross-coupling reactions (e.g., amination of organic halides) [1,3] and for the activation of O_2 and C–H bonds [2]. Complexes of Pd(I) are rare: a search in the Cambridge Structure Database revealed that, although a vast number of palladium oligomers have been characterised structurally, fewer than 25 structures belong to com-

plexes that can be formally regarded as Pd(I) species [10–20,4,21–31].

We have been studying differences in the reactivity of imino- and keto-phosphine ligands from that of the amido-phosphine ligand, when coordinated to transition metals such as Mo(II) [32], Rh(I) [33], Ni(II) [34], Pd(II) [35] or Pt(II) [34]. We have demonstrated an unprecedented hydrogen–deuterium exchange of methylene and olefinic protons in coordinated neutral or anionic ketophosphine ligands $[\text{Ph}_2\text{PCH}_2\text{C}(\text{Ph})=\text{O}]$ and $[\text{Ph}_2\text{PCHC}(\text{Ph})\text{O}]^-$ [32]. Leung and co-workers have also observed an imine–enamine tautomerism as a result of the D_2O addition to a CDCl_3 solution of a related Pd(II) iminophosphine complex [36].

We have recently shown that the reaction between $[\text{PdBr}_2\{\text{Ph}_2\text{PCH}_2\text{C}(\text{Ph})=\text{N}(2,6\text{-Me}_2\text{C}_6\text{H}_3)\}]$ and MeLi in THF gives mainly the dimer $[\text{Pd}_2(\mu\text{-Br})_2\{\text{Ph}_2\text{PCH}=\text{C}(\text{Ph})\text{N}(2,6\text{-Me}_2\text{C}_6\text{H}_3)\}_2]$; when reacted with MeLi deprotonation of the CH_2 group of the ligand backbone seems to be favoured over the alkylation of the Pd(II) centre [35]. We report here the formation and structural elucidation

^{*} Corresponding authors.

E-mail address: jennifer.green@chem.ox.ac.uk (J.C. Green).

¹ Present address: Chemistry Research Laboratory, University of Oxford, 12 Mansfield Road, Oxford, OX1 3TA, UK.

of new Pd(I) species and describe their significance to the CO/ethylene copolymerisation mechanism reaction catalysed by Pd(II)–amidophosphines or enolisable Pd(II)–iminophosphines.

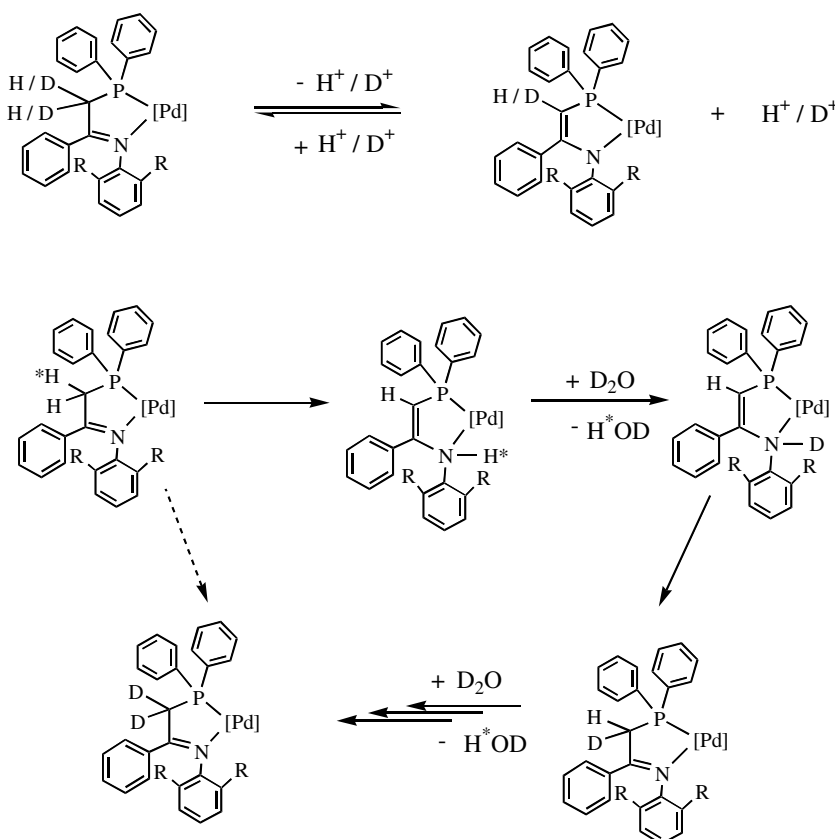
2. Results and discussion

2.1. Synthesis and spectroscopy

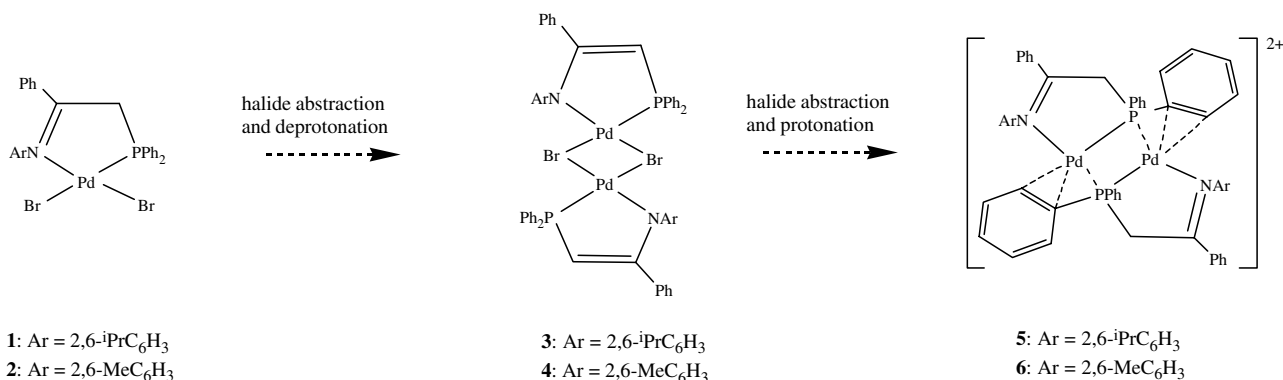
We followed the imine–enamine exchange in mononuclear Pd(II) complexes $[\text{PdBr}_2\{\text{Ph}_2\text{PCH}_2\text{C}(\text{Ph})=\text{N}(2,6\text{-}^i\text{Pr}_2\text{C}_6\text{H}_3)\}]$ (**1**) and $[\text{PdBr}_2\{\text{Ph}_2\text{PCH}_2\text{C}(\text{Ph})=\text{N}(2,6\text{-Me}_2\text{C}_6\text{H}_3)\}]$ (**2**) (prepared following established procedures [34,35] by ^1H NMR experiments (CD_2Cl_2 , r.t.)). Spectra were measured after treating each of these samples with one equivalent of CD_3OD . The resonance signals characteristic of the $\text{CH}_2\text{-P}$ protons of the Pd-coordinated ligand (at δ 4.45 for complex **1**, δ 4.24 for complex **2**) [34,35] disappeared almost immediately upon adding d^4 -methanol or D_2O to the corresponding samples. The other regions of the ^1H NMR spectra remained unchanged and no significant modifications in the chemical shifts of the aromatic and methyl protons were observed. No decomposition was observed after standing for two days at room temperature, even following exposure of the solutions to air. The bidentate ligand is likely to be susceptible to rapid imine–enamine tautomerism, since C–H protons in the

imino-form are generally expected to be inert to H/D exchange but N–H protons in the enamino form are prone to exchange. The $^{31}\text{P}\{^1\text{H}\}$ NMR spectra of the samples showed the original singlet signals throughout the course of experiment. Imine–enamine tautomerism takes place faster than the NMR chemical shift scale in solution at room temperature. A simple equilibrium between protonated and deprotonated forms of the complexes, involving the intramolecular imine–enamine transformations, explains this exchange (Scheme 1).

As a result of these observations, we have tested the acidity of the methylene backbone in $[\text{PdBr}_2(\text{HL1})]$ (**1**) and $[\text{PdBr}_2(\text{HL2})]$ (**2**) by treating these with strong bases such as MeLi and KH in THF at -78°C . The reactions with KH proceeded cleanly and in high yield, to give Pd(II) amidophosphine dimers $[\text{Pd}_2(\mu\text{-Br})_2\{\text{Ph}_2\text{PCH}=\text{C}(\text{Ph})\text{N}(2,6\text{-R}_2\text{C}_6\text{H}_3)\}_2]$, where $\text{R} = ^i\text{Pr}$ (**3**) and Me (**4**) (Scheme 2) as moderately air- and moisture-sensitive green powders. Earlier studies showed the facile conversion of M-coordinated enamino–phosphines to the parent M-ketophosphines [32]. The treatment of CD_2Cl_2 solutions of **3** and **4** with degassed CD_3OD or D_2O gave complex mixtures of species. Indeed, ^1H NMR experiments indicated that conversion of the Pd-coordinated amidophosphine back to its iminophosphine form could take place whilst the ligand remained metal-coordinated. (*N.B.* The doublet characteristic to δ_{CHP} at ca. 3.54 ppm was replaced by broad signals



Scheme 1. Proposed mechanism for the H/D exchange of **1** and **2** in $\text{CD}_2\text{Cl}_2/\text{MeOD}$ solutions.

Scheme 2. Overall transformation process from the Pd(II) complexes **1** and **2** to the Pd(I) complexes **5** and **6**.

at ca. 4.2 ppm; this is within the range expected for $\delta_{\text{CH}_2\text{P}}$ in the related iminophosphines **1** and **2**.

When compounds $[\text{Pd}_2(\mu\text{-Br})_2\{\text{Ph}_2\text{PCH}=\text{C}(\text{Ph})\text{N}(2,6\text{-R}_2\text{C}_6\text{H}_3)\}]_2$, where R = ⁱPr (**3**) and Me (**4**) were treated with two equivalents of AgBF_4 in CH_2Cl_2 in presence of MeOH, the corresponding iminophosphine dimers $[\text{Pd}\{\text{Ph}_2\text{PCH}_2\text{C}(\text{Ph})=\text{N}(2,6\text{-R}_2\text{C}_6\text{H}_3)\}]_2[\text{BF}_4]_2$, where R = ⁱPr (**5**) and Me (**6**), were isolated as air and moisture stable yellow-orange crystals. The reaction yields were lower than 15% in each case, and a series of intractable decomposition species and Pd metal were also present. The overall transformation process from the neutral Pd(II) complexes **1** and **2** to the Pd(I) dicationic species **5** and **6** is outlined in Scheme 2.

For dimers **5** and **6**, the formal oxidation state of Pd is I and the valency number [37] is 2. ¹H NMR spectroscopy (CD_2Cl_2) of **6** shows broad signals: the resonance at δ 2.30 corresponds to the Me protons of the *N*-xylyl unit, the doublet at δ 5.17 ($^2J_{\text{PH}} = 13.4$ Hz) to the $\text{CH}_2\text{-P}$ protons of the ligand and the aromatic protons were observed as broad multiplets in the region δ 7.61–6.80. All *Ph*-P groups appear equivalent on the NMR timescale at room temperature, suggesting that the aromatic rings are not involved in chemical bonding with the unsaturated Pd-centre or are undergoing rapid exchange. ³¹P NMR spectroscopy of **6** shows a singlet (δ 47.9 in CD_2Cl_2 or δ 49.4 in CDCl_3), indicating that the two P nuclei are magnetically equivalent in solution. ¹³C NMR spectroscopy (CD_2Cl_2) showed only one type of phenyl for the *PPh*₂ groups. ¹¹B NMR spectroscopy (CD_2Cl_2) shows a singlet at δ -0.2 only, and ¹⁹F NMR spectroscopy shows a single resonance, at δ -150.0. The latter chemical shift indicates that the fluorine atoms of the BF_4 units are not part of the coordination sphere of the Pd atoms. Similar features in the NMR spectra of **5** were found, and these are listed in Section 5.

Molecular structure determination by X-ray diffraction showed that **6** is a coordinatively unsaturated formally Pd(I) dimer where the $\text{Pd}_2\text{N}_2\text{P}_2$ system deviates from planarity (vide infra) by ca. 14°. We believe that this dimer is formed from the Pd(0) and Pd(II) species $[\text{Pd}\{\text{Ph}_2\text{PCH}_2\text{-C}(\text{Ph})=\text{N}(2,6\text{-Me}_2\text{C}_6\text{H}_3)\}]$ and $[\text{Pd}\{\text{Ph}_2\text{PCH}_2\text{C}(\text{Ph})=\text{N}(2,6\text{-Me}_2\text{C}_6\text{H}_3)\}]^{2+}$ by the pathway described in Scheme 3.

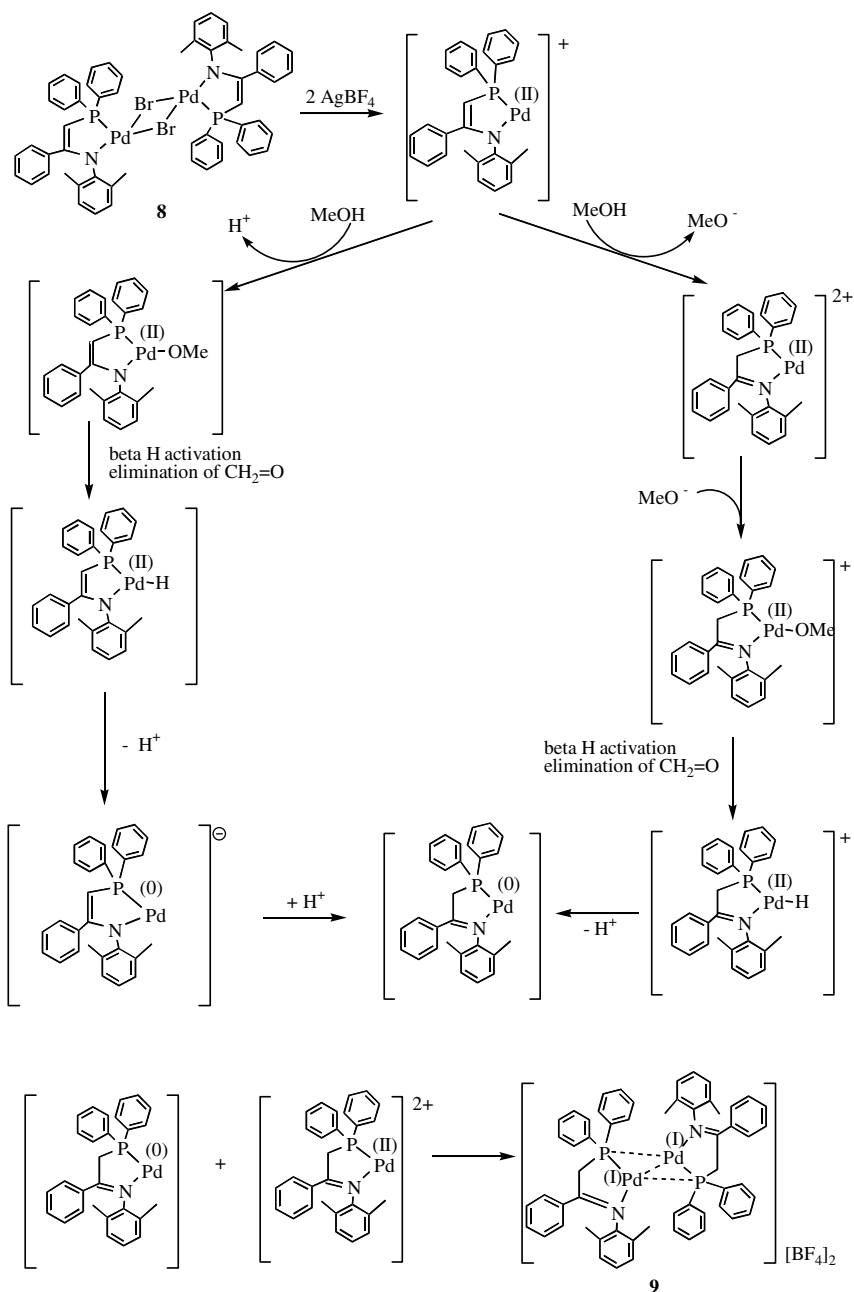
MeOH could act as the protonating agent for chelating anionic ligands of the type $\text{L}^- = [\text{Ph}_2\text{PCH}=\text{C}(\text{Ph})\text{N}(2,6\text{-R}_2\text{C}_6\text{H}_3)]^-$ (3 electron donors) in $[\text{Pd}(\text{L}^-)]^{2+}$. This would lead to formation of a $[\text{Pd}(\text{HL})]^{2+}$ species, where the neutral ligand $\text{HL} = [\text{Ph}_2\text{PCH}_2\text{C}(\text{Ph})=\text{N}(2,6\text{-R}_2\text{C}_6\text{H}_3)]$ (a four-electron donor). A similar route was proposed previously by Budzelaar and co-workers for the formation of $[\text{Pd}(\text{dppp})]_2[\text{SO}_3\text{CF}_3]_2$, where *dppp* = 1,3-bis(diphenylphosphino)propane [27]. The effect of MeOH as the activator for formation of the Pd(II)-dications is believed to be an important step in the mechanism for CO–ethylene copolymerisation catalysed by Pd(II) chelating diphosphines. Here, it may result in the in situ formation of initiator species such as $[\text{Pd}(\text{HL})(\text{OMe})]^{2+}$, where $\text{HL} = [\text{Ph}_2\text{PCH}_2\text{C}(\text{Ph})=\text{N}(2,6\text{-R}_2\text{C}_6\text{H}_3)]$, which can undergo β -hydride elimination leading to formation of a hydride initiator $[\text{Pd}(\text{HL})\text{H}]^{2+}$ and subsequently give a $[\text{Pd}^{(0)}(\text{HL})]$ species by reductive elimination. The resulting H^+ can then re-enter the catalytic cycle as a protonating reagent for the enamine ligand. In the established CO–ethylene polymerisation mechanism using (*dppp*)-Pd(II) catalyst systems in MeOH, chains are generally terminated by reaction of MeOH with the various propagating species, to produce new initiators (Pd(II)–hydride monocations) in the chain transfer processes [38]. In the chain termination process these Pd(II)–hydride monocationic intermediates are subsequently deactivated by decomposition to Pd(0) species, which can combine with Pd(II)dicationic species to form dicationic Pd(I)-dimers. Indeed, when compounds **3** and **4** were tested for activity in the CO/ethylene copolymerisation process in the presence of MeOH and AgBF_4 , complexes **5** or **6** could also be isolated from the autoclave.

2.1.1. Molecular structures of

$[\text{Pd}_2\text{Br}_2(\text{Ph}_2\text{PCH}=\text{C}(\text{Ph}))\text{N}(2,6\text{-R}_2\text{C}_6\text{H}_3)]$, R = ⁱPr (**3**) and Me (**4**)

ORTEP diagrams for molecular structures of **3** and **4** are shown in Figs. 1 and 2 and relevant molecular parameters are given in Table 1.

Complex **3** crystallises with one molecule of CH_2Cl_2 , as blue-purple needle-like crystals. The complex $[\text{Pd}_2(\mu\text{-Br})_2(\text{L}_2)_2]$ (**4**) crystallises from a purple CH_2Cl_2 solution as a



Scheme 3. Proposed mechanism for the formation of $[\text{Pd}\{\text{Ph}_2\text{PCH}_2\text{C}(\text{Ph})=\text{N}(2,6\text{-Me}_2\text{C}_6\text{H}_3)\}]_2[\text{BF}_4]_2$ where $\text{R} = \text{tPr}$ (**5**), Me (**6**).

mixture of two polymorphs. The green plates crystals of **4a** (reported elsewhere) [35] were the major species. The thin, purple needle-like crystals of **4b** were the minor species and these appeared after the concentrated CH_2Cl_2 solution of **4** was kept at -20°C for several weeks. The final ratio of **4a**:**4b** was approximately 4:1. X-ray crystallography showed that in the case of **4a**, $[\text{Pd}_2(\mu\text{-Br})_2(\text{L}2)_2]$ crystallises together with two molecules of CH_2Cl_2 , whereas **4b** is non-solvated. The geometries around the palladium centres of **3** and **4** are essentially square-planar. Changes in the structure of the ligands are reflected in the molecular parameters of the complexes. The bond lengths determined for the C–C backbones in **3**, **4a** and **4b** (i.e., 1.373(11), 1.379(4) and

1.381(9) Å, respectively) are considerably shorter than those found for the neutral free ligand **HL2** (1.504 Å) or for the metal-coordinated ligands in $[\text{PdBr}_2(\text{HL}1)]$ (**1**) and $[\text{PdBr}_2(\text{HL}2)]$ (**2**) (1.51(1) and 1.502(3) Å, respectively). Shorter carbon–carbon bonds of the ligand backbone in **3** and **4** (**a** and **b**) are consistent with the formation of a double bond as a result of the deprotonation of the coordinated neutral ligand in the presence of a base. In addition, the carbon(backbone)–nitrogen distances are significantly greater in **3** (1.368(9) Å), **4a** (1.351(4) Å) and **4b** (1.371(8) Å) than those found in the Pd-coordinated neutral ligands, which are 1.290(9) Å in $[\text{PdBr}_2(\text{HL}1)]$ (**1**) and 1.292(3) Å in $[\text{PdBr}_2(\text{HL}2)]$ (**2**) [34,35]. This is consistent

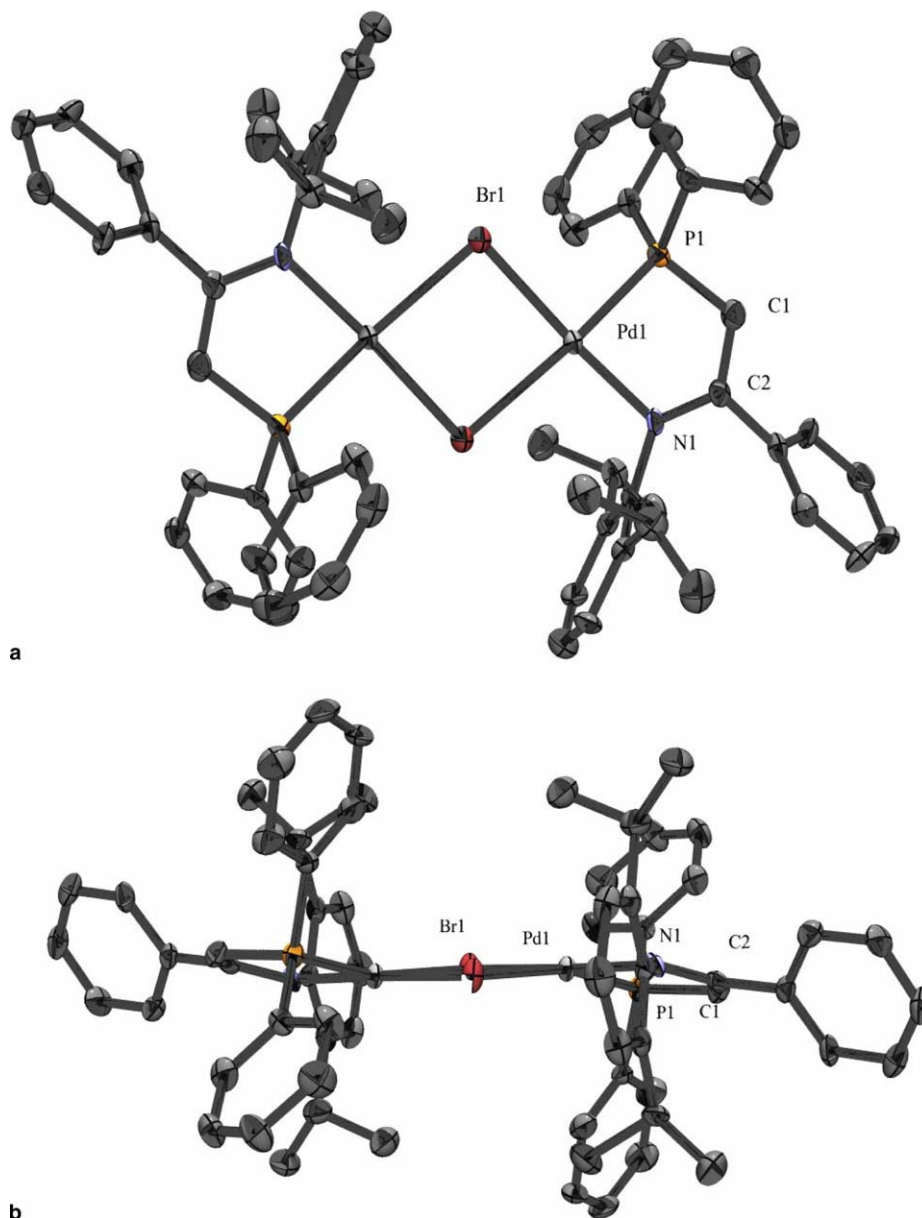


Fig. 1. (a) ORTEP diagram of the molecular structure of complex **3**. (b) Alternative view of the molecular structure of complex **3b** (ORTEP diagrams showing the planar four-member ring).

with a decrease in the C–N bond order as a result of deprotonation and imine–enamine tautomerisation. In **3** and **4** (**a** and **b**), the Pd–Br distances *trans* to phosphorus are somewhat longer than the corresponding bonds *cis* to phosphorus reflecting the greater *trans* influence of phosphorus compared to nitrogen (Table 1). The palladium–palladium separation in the planar, non-solvated, species **4b** is 3.7206(1)° whereas in the (bent) solvated species **4a** it is considerably shorter (3.397(1) Å). For the planar molecule **3**, this distance is also 3.691(1) Å. The palladium and bromine centres form inorganic four-member rings. The ring is distorted from planarity (with a dihedral angle Pd1–Br1–Pd1'–Br1' of 130.08°) in **4a**, and essentially planar in **4b** and **3**. It was noted that the P–Pd–N bite angles for

4a (83.62(8)°) and **4b** (83.70(15)°) are slightly larger than for [PdBr₂(HL2)] (**2**) (82.91(6)°). For **3**, this angle measures 83.94(18), compared to its mononuclear precursor [PdBr₂(HL2)] (**1**), where this angle measured 81.16(16)°. Interestingly, **4b** shows a dihedral angle Br(1)–Pd(1)–Br(1)'–Pd(1)' of almost 0° and the inter-planar angles [Pd(1)/P(1)/C(1)]–[Pd(1)/N(1)/C(2)/C(1)] and [P(1)/Pd(1)/N(1)]–[Br(1)–Pd(1)–Br(1)'] of 6.6° and 5.7°, respectively. Complex **4a** showed a more buckled geometry, with a dihedral angle Br(1)–Pd(1)–Br(1)'–Pd(1)' of 47.4°, and inter-planar angles [Pd(1)/P(1)/C(1)]–[Pd(1)/N(1)/C(2)/C(1)] and [P(1)/Pd(1)/N(1)]–[Br(1)–Pd(1)–Br(1)'] of 6.3° and 7.2°, respectively. Differences between the overall geometries of the two polymorphs occur as a result of the fact that, in the case of **4a**,

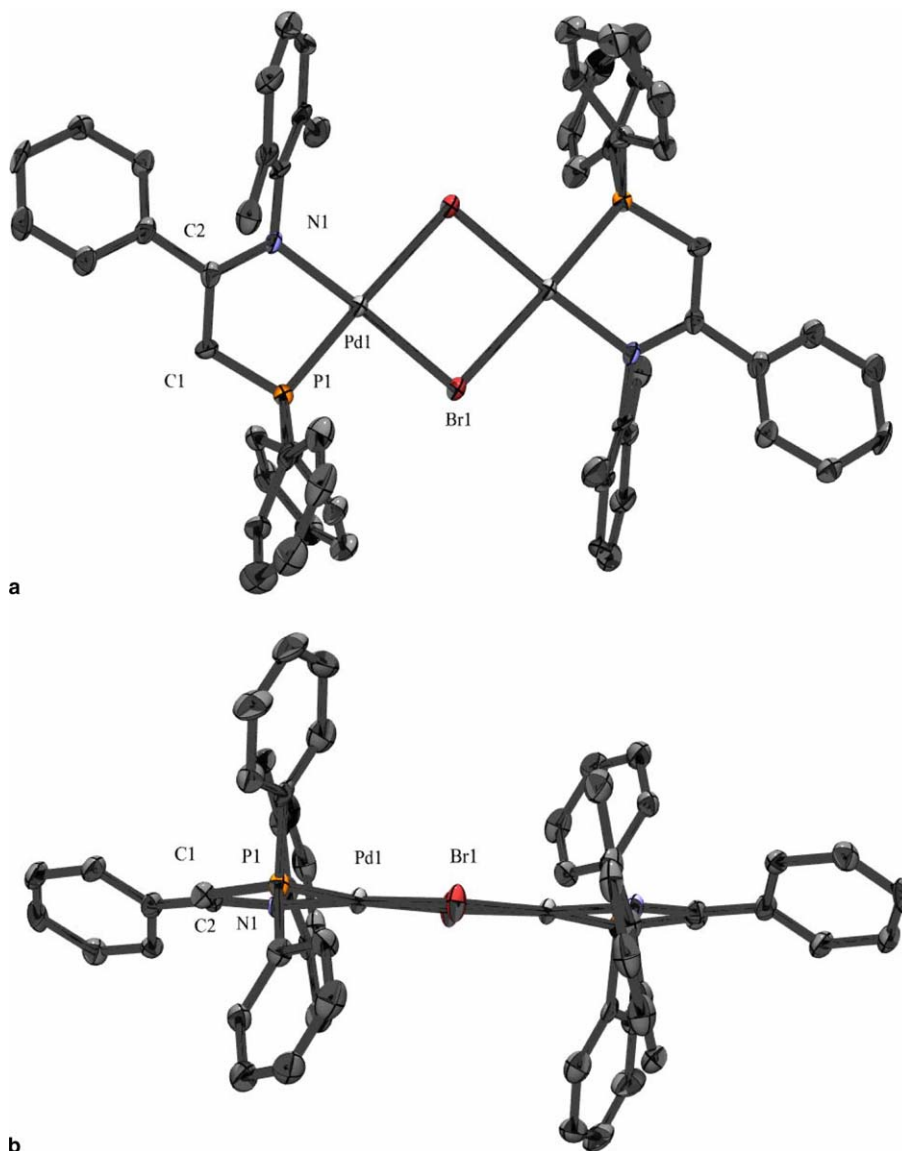


Fig. 2. (a) ORTEP diagram of the molecular structure of complex **4b**. (b) Alternative view of the molecular structure of complex **4b**. (ORTEP diagram showing the planar four-member ring.)

the molecule is folded and forms a ‘cavity’, which accommodates the two molecules of CH_2Cl_2 .

2.1.2. Molecular structure of **6** and bonding in Pd(I) dimers **5** and **6**

The crystal structure determination shows that the complex **6** is a dicationic Pd(I) dimer. The asymmetric unit contains one half of the molecule **6**, therefore half of the cation shown in Fig. 3(a) is symmetry-generated. The X-ray structure confirmed that compound **6** is a dimer with the PPh_2 unit bridging two palladium atoms. The Pd–Pd distance in **6** (2.7411(8) Å) is close to that observed for the dimer $[\text{dppp}]\text{Pd}_2(\text{SO}_3\text{CF}_3)_2$ (2.701(3) Å), which also shows a PPh_2 unit bridging two palladium atoms as a result of ‘side-on’ interactions. A search in the Cambridge Structural Database indicated that the Pd–Pd bond length of compound **6** is situated in the middle of the range for

Pd–Pd distances in Pd-dimers, suggesting a Pd–Pd single bond. Several other examples of Pd(I) dimers have been reported, however bridging Pd– PPh_2 –Pd interactions of the type observed for **6** are rare [39]. Each Pd centre of **6** is coordinated by one $[\text{Ph}_2\text{PCH}_2\text{C}(\text{Ph})=\text{N}(2,6\text{-Me}_2\text{C}_6\text{H}_3)]$ ligand in which the phosphorus atom occupies an (asymmetrically) bridging position.

The Pd– C_{ipso} and Pd– C_{ortho} distances between each palladium atom and one of the P-aryl groups belonging to the ligand coordinated to the other palladium atom are short (2.363(5) and 2.58 Å, respectively), suggesting a delocalised Pd–P– C_{ipso} – C_{ortho} interaction in the solid state involving only one of the aromatic rings of each of the PPh_2 units. The lengths of the two P– C_{ipso} bonds within a given PPh_2 (P(1)–C(17) = 1.815(5) Å and P(1)–C(23) = 1.826(5) Å) are slightly different. However, the fact that all the respective bond lengths and bond angles of the first aromatic ring

Table 1
Selected bond lengths and bond angles for complexes **3**, **4** (polymorph **b**) and **6**

Compound	Bond lengths (Å)		Bond angles (°)	
3	Pd(1)–Br(1)'	2.5881(9)	Br(1)'–Pd(1)–Br(1)	85.27(3)
	Pd(1)–P(1)	2.2098(19)	Br(1)'–Pd(1)–P(1)	167.61(6)
	Pd(1)–Br(1)	2.4528(10)	Br(1)–Pd(1)–P(1)	92.85(6)
	Pd(1)–N(1)	2.046(6)	Br(1)'–Pd(1)–N(1)	98.37(17)
	N(1)–C(21)	1.418(9)	Br(1)–Pd(1)–N(1)	176.02(18)
	N(1)–C(2)	1.368(9)	P(1)–Pd(1)–N(1)	83.94(18)
	P(1)–C(15)	1.814(8)		
	P(1)–C(9)	1.807(7)		
	P(1)–C(1)	1.753(8)		
	C(1)–C(2)	1.373(11)		
	4b^a	Pd(1)–Br(1)	2.4728(7)	Br(1)–Pd(1)–Br(1)'
Pd(1)–Br(1)'		2.5703(8)	Br(1)–Pd(1)–P(1)	93.22(5)
Pd(1)–P(1)		2.2023(15)	Br(1)'–Pd(1)–P(1)	175.56(6)
Pd(1)–N(1)		2.040(5)	Br(1)–Pd(1)–N(1)	175.17(16)
P(1)–C(1)		1.731(6)	Br(1)'–Pd(1)–N(1)	98.40(14)
P(1)–C(17)		1.806(6)	P(1)–Pd(1)–N(1)	83.70(15)
P(1)–C(23)		1.814(6)	Pd(1)–Br(1)–Pd(1)'	95.06(3)
C(1)–C(2)		1.381(9)	Pd(1)–P(1)–C(1)	102.5(2)
C(2)–N(1)		1.371(8)	Pd(1)–N(1)–C(2)	118.2(4)
C(3)–N(1)		1.417(8)	Pd(1)–N(1)–C(3)	118.0(4)
6		Pd(1)–Pd(1)'	2.7411(8)	N(1)–Pd(1)–P(1)'
	P(1)–C(23)	1.826(5)	Pd(1)'–Pd(1)–N(1)	138.99(11)
	C(1)–C(2)	1.512(7)	Pd(1)'–Pd(1)–P(1)	57.14(4)
	P(1)–C(17)	1.815(5)	N(1)–Pd(1)–P(1)	82.62(12)
	P(1)–C(2)	1.822(5)	Pd(1)'–Pd(1)–P(1)'	51.11(3)
	N(1)–C(1)	1.288(7)	P(1)'–Pd(1)–C(23)'	44.83(13)
	Pd(1)–C(23)'	2.363(5)	Pd(1)'–C(23)–C(24)	82.6(3)
	Pd(1)–P(1)'	2.4243(15)	Pd(1)'–C(23)–P(1)	69.37(17)
	Pd(1)–P(1)	2.2466(13)	Pd(1)'–P(1)–C(23)	65.80(17)
	Pd(1)–N(1)	2.135(4)	Pd(1)–P(1)–C(23)	131.46(18)
			P(1)–Pd(1)–P(1)'	108.25(4)
			Pd(1)'–Pd(1)–C(23)'	93.19(13)
			P(1)–Pd(1)–C(23)'	146.42(14)
			Pd(1)–N(1)–C(1)	118.9(4)
			Pd(1)–N(1)–C(9)	118.7(3)
			Pd(1)–P(1)–Pd(1)'	71.75(4)
			N(1)–Pd(1)–C(23)'	127.70(17)

^a Selected molecular parameters found for polymorph **4a** (reported earlier) [35] C(1)–C(2) 1.379(4), Pd(1)–Br(1) 2.4629(4), Pd(1)–Br(1)' 2.5655(4), C(2)–N(1) 1.351(4), C(3)–N(1) 1.424(4) Å and Br(1)–Pd(1)–Br(1)' 84.937(14), Br(1)–Pd(1)–P(1) 93.77(2), Br(1)'–Pd(1)–P(1) 176.87(3)°. **4a** contains one molecule of CH₂Cl₂ in the asymmetric unit.

are extremely close to those of the second, and similar to those expected for an uncoordinated phenyl ring, raises a question about the hypothesis of a delocalised Pd–P–C_{ipso}–C_{ortho} interaction between one of the PPh₂ aromatic rings and the coordinatively unsaturated Pd centre in the solid state (as indicated by the dotted lines in Fig. 3(a)).

The Pd(1)'–Pd(1)–P(1) and Pd(1)–P(1)–Pd(1)' angles are acute (57.14(4)° and 71.75(4)°, respectively) and somewhat larger than the corresponding angles for [(dppp)Pd]₂–(SO₃CF₃)₂ (49.0(1)° and 65.2(1)°). The Pd and N atoms occupy positions forming an almost linear arrangement N–Pd–Pd–N, and the angle P(1)'–Pd(1)–N(1) is 166.46(2). The bond lengths determined for the C–C backbones of **6** (1.512(7) Å) are considerably longer than the corresponding bonds for compound **4**, [Pd₂(μ-Br)₂{Ph₂PCH=C(Ph)N(2,6-Me₂C₆H₃)₂}₂]⁻ (1.379(4) Å in the di-solvated molecule **4a** and 1.381(9) Å in the non-solvated species **4b**), and are similar to those found for the neutral (free or coordinated to

PdX₂ units, X = Cl, Br, I) ligand [Ph₂PCH₂C(Ph)=N(2,6-Me₂C₆H₃)] (**HL2**). The fact that the ligand backbone carbon–carbon bonds of **6** are significantly longer than those of **4a** and **4b** is consistent with the formation of a single bond upon protonation of the coordinated anionic ligand of **4**. In addition, the carbon(backbone)–nitrogen distances (1.288(7) Å) are significantly shorter for **6** than for **4a** (1.351(4) Å) and **4b** (1.371(8) Å) and close to those found in the free ligand [Ph₂PCH₂C(Ph)=N(2,6-Me₂C₆H₃)] (**HL2**) or coordinated to Pd(II) in complexes **1** and **2** [34,35]. This is consistent with an increase in the C–N bond order as a result of protonation and enamine–imine tautomerisation and also, therefore, with the observation that in [Pd{Ph₂PCH₂C(Ph)=N(2,6-Me₂C₆H₃)₂}₂][BF₄]₂ (**6**) the ligands exist in an iminophosphine form. Table 1 shows the significant bond lengths and bond angles for [Pd{Ph₂PCH₂C(Ph)=N(2,6-Me₂C₆H₃)₂}₂][BF₄]₂ (**6**). The Pd(1)–P(1)–Pd(1)'–P(1)' cycle is planar by symmetry, and

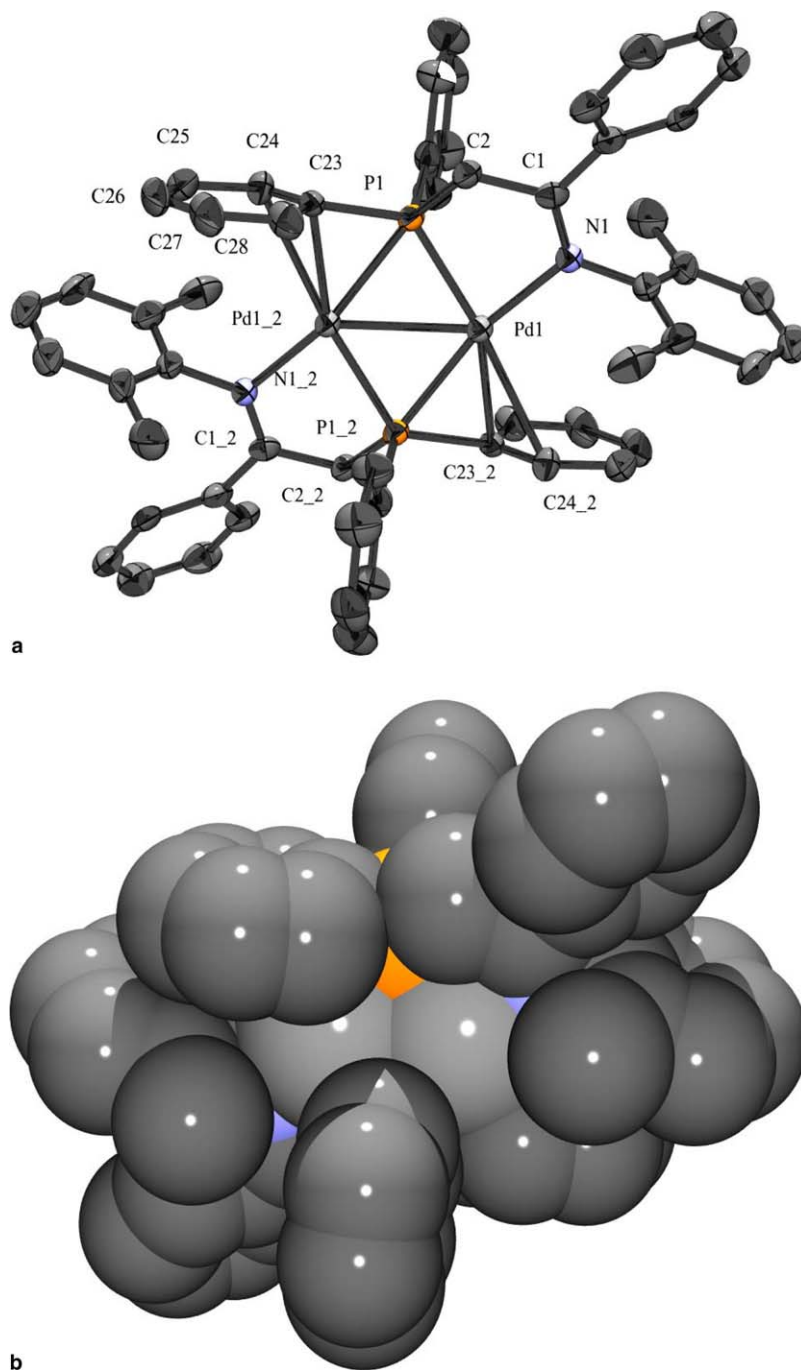


Fig. 3. (a) ORTEP diagram showing the dicationic unit $\text{Pd}\{\{\text{Ph}_2\text{PCH}_2\text{C}(\text{Ph})=\text{N}(2,6\text{-Me}_2\text{C}_6\text{H}_3)\}\}_2^{2+}$ in **6**. (All the H atoms and the two $[\text{BF}_4]^-$ units were excluded for clarity.) (b) Space-filling model of the dication unit in **6**.

the $[\text{Pd}(1)/\text{P}(1)\text{P}(1)']\text{--}[\text{P}(1)\text{--Pd}(1)/\text{N}(1)]$ inter-planar angle is 8.3° . The two 5-membered chelate rings incorporating the Pd(1) and Pd(1') atoms, respectively, are identical by symmetry and moderately buckled, with an inter-planar angle $[\text{Pd}(1)/\text{P}(1)/\text{C}(2)]\text{--}[\text{Pd}(1)/\text{N}(1)/\text{C}(1)/\text{C}(2)]$ of 33° . Furthermore, the 3D structure of **6** shows mutually reinforcing non-covalent interactions such as (intramolecular) $\pi\text{--}\pi$ stacking of the Ph(C) ring and the aryl-imine belonging to adjacent monomer units, and extended intermolecular

B–F...H–C interactions between BF_4 counterions and aromatic hydrogens of PPh_2 groups.

2.1.3. DFT calculations

The apparent coordination of a phenyl group to the opposing Pd raises the question as to whether it is crucial to the dimerisation. In order to understand the nature of the dimeric structure of the compound **6**, density functional calculations were carried out on model-compounds, where

the coordinating phenyl groups were present and absent. The phenyl groups outside the coordination sphere of the palladium atoms were substituted by hydrogen atoms to reduce computational time. Geometry optimisations were carried out for the species shown in Fig. 4. The absence of coordinating phenyl groups was modelled with both a chelating ligand in $[\text{Pd}(\text{H}_2\text{PCH}_2\text{CH}=\text{NH})]^+$ (**I**) and $[\text{Pd}_2(\text{H}_2\text{PCH}_2\text{CH}=\text{NH})_2]^{2+}$ (**II**), and monodentate imine and phosphine ligands simultaneously coordinated to the metal in $[\text{Pd}(\text{H}_3\text{P})(\text{NH}=\text{CH}_2)]^+$ (**I'**) and $[\text{Pd}_2(\text{H}_3\text{P})_2(\text{NH}=\text{CH}_2)]^{2+}$ (**II'**). Both linear and bent geometries (**I'a** and **I'b**, respectively) were modelled for $[\text{Pd}(\text{H}_3\text{P})(\text{NH}=\text{CH}_2)]^+$ (**I'**). To ascertain the effect of an aryl substituent of the bridging phosphine on the overall geometry, geometry optimisations were also carried out for $[\text{Pd}\{\text{H}(\text{Ph})\text{P}=\text{CH}_2-$

$\text{CH}=\text{NH}\}]^+$ (**I''**) and $[\text{Pd}_2\{\text{H}(\text{Ph})\text{PCH}_2\text{CH}=\text{NH}\}_2]^{2+}$ (**II''**) (Fig. 4). All these models were optimised without symmetry constraints. Scheme 4 shows the estimated energies for the dimerisation reactions: **I** \rightarrow **II**, **I'** \rightarrow **II'** and **I''** \rightarrow **II''**. These energies would of course best model the internal energy in a gas-phase reaction. As observed from Scheme 4, compound **II''** is more stable with respect to the monomers than compounds **II** and **II'**, but this could also be due to the fact that charge is more dispersed in this larger complex.

As expected, the models including chelating N/P ligands are energetically more easily dimerised than the models containing the non-chelating phosphine and imine ligands. The monomer **I'** (formally a d^9 radical) favours a linear structure (as in **I'a**) but initial bending (to **I'b**) is necessary to form the dimer **II'**. The estimated energy differences for

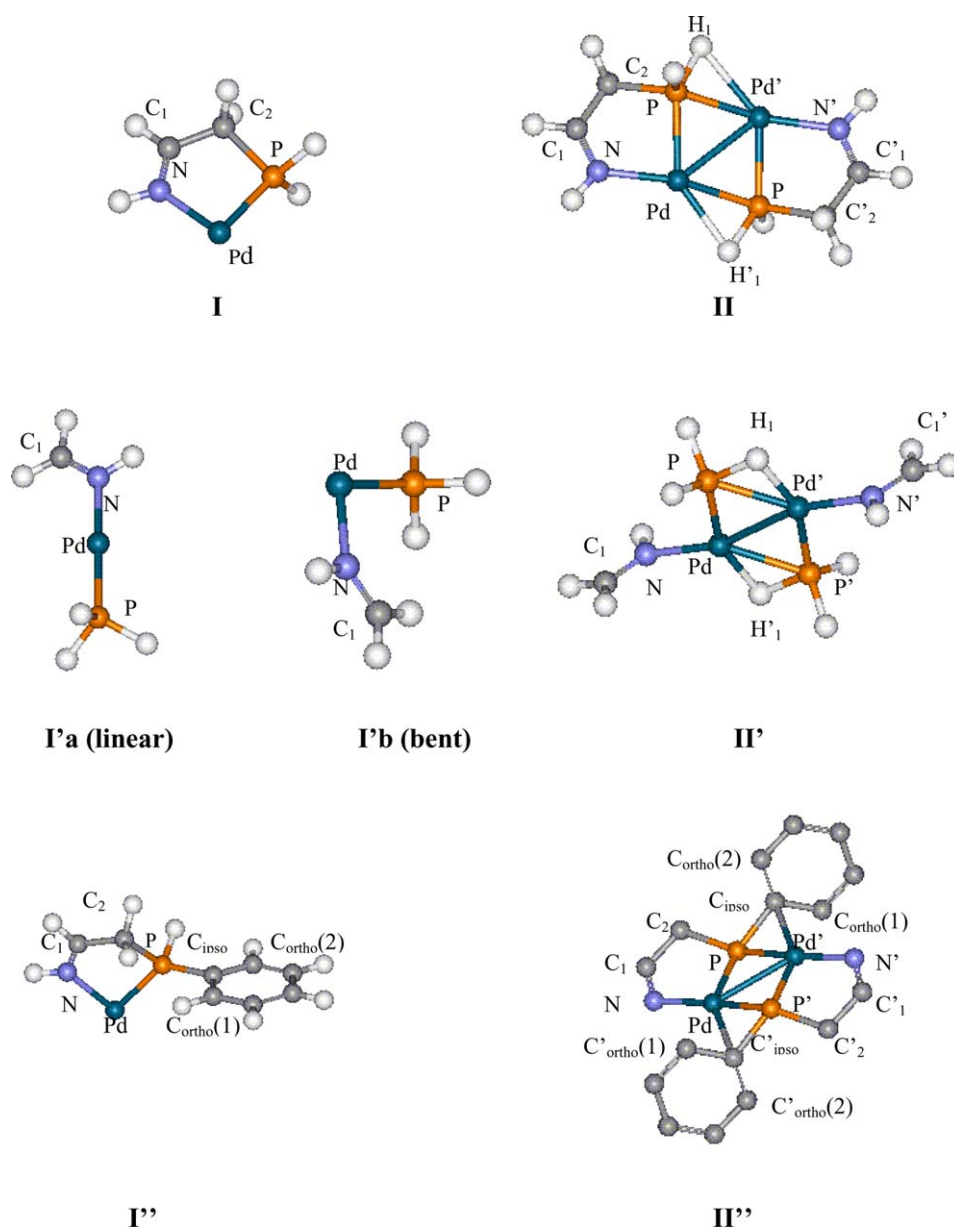
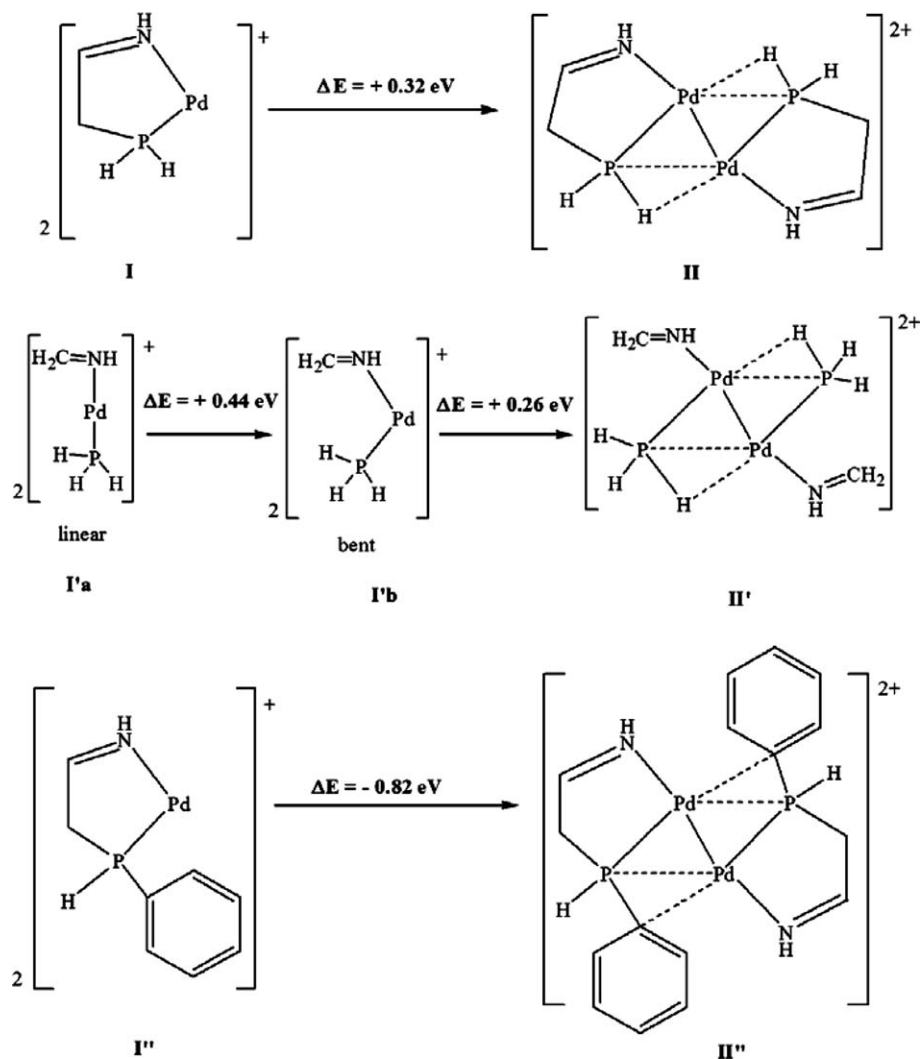


Fig. 4. Optimised geometries for the monocationic species **I**, **I'** (**a** and **b**) and **I''** and the dicationic species **II**, **II'** and **II''**. (In the representation of model-compound **II''** all H atoms have been removed for clarity.)



Scheme 4. Energies of formation and dimerisation energies for the monocationic species **I**, **I'** (a and b), **I''** and the dicationic species **II**, **II'** and **II''**.

the dimerisation reactions of **I**, **I'** and **I''** indicate that the dimerisation of **I''** is considerably more energetically favoured than the dimerisation reactions of **I** and **I'**. These results suggest that the presence of the phenyl ring at the bridging phosphine is essential for stabilising the resulting dicationic dimer.

Geometry optimisations produced calculated values for bond lengths, inter-atomic distances and angles. The results of these geometry optimisations for the monocations **I**, **I'** (a and b) and **I''** and for the dications **II**, **II'** and **II''** are given in Table 2, together with experimental values (from the X-ray structure of **6**). Reasonable agreement with the crystal structure confirms that the models **II**, **II'** and **II''** work well despite of the absence of phenyl groups. The presence of only one phenyl group at the P donor (in **II''**) was found to make very little difference to the bond angles and lengths around the Pd-centre. Also, although non-chelating ligands are used in **II'**, the metal–ligand interatomic distances are in reasonable agreement with the values obtained from the crystal structure of **6**. DFT optimised structures have shown short bond lengths both between the palladium

and hydrogen atoms of the bridging phosphine (in **II** and **II'**) and between the palladium and phenyl *ipso* carbons of the bridging phosphines (in **II''**) (Table 2). Carbon–carbon bond distances (from crystal structure) within the phenyl rings of interest from the crystal structure of $[\text{Pd}\{\text{Ph}_2\text{PCH}_2\text{C}(\text{Ph})=\text{N}(2,6\text{-Me}_2\text{C}_6\text{H}_3)\}_2][\text{BF}_4]_2$ (**6**), together with the corresponding values calculated for $[\text{Pd}_2\{\text{H}(\text{Ph})\text{PCH}_2\text{CH}=\text{NH}\}_2]^{2+}$ (**II''**) are shown in Fig. 5. DFT calculations showed only relatively small differences between C–C bonds within a phenyl group. However, a tendency towards the redistribution of π -electron density inside the aromatic ring is suggested for the aromatic ring attached to the phosphorus atom (involved in the ‘side-on’ interaction with the Pd-centre) in **II'**. Therefore, the existence of a bonding interaction involving the phenyl ring of the P(Ph)H group is indicated in the gas phase.

The inspection of the frontier orbitals in **II**, **II'** and **II''** was necessary in order to help understand the nature of the bonding in complex **6**. Fig. 6 shows the energy diagrams of frontier molecular orbitals for these models and Fig. 7(a)–(c) shows the shapes of selected molecular orbitals.

Table 2
Experimental and calculated bond lengths and bond angles for dications **6**, **II**, **II'** and **II''**^a

Bond distances (Å)	6	II	II'	II''
Pd–Pd'	2.7411(8)	2.708	2.627	2.751
Pd–N (Pd'–N')	2.135(4)	2.061 (2.058)	2.029 (2.030)	2.066 (2.067)
Pd–P (Pd'–P')	2.2466(13)	2.277 (2.269)	2.260 (2.262)	2.256 (2.257)
Pd–P' (Pd'–P')	2.4243(15)	2.262 (2.287)	2.321 (2.317)	2.422 (2.426)
C ₁ –N (C' ₁ –N')	1.288(7)	1.278 (1.278)	1.271 (1.271)	1.278 (1.278)
C ₁ –C ₂ (C' ₁ –C' ₂)	1.512(7)	1.475 (1.476)		1.473 (1.473)
P–C ₂ (P'–C' ₂)	1.822(5)	1.853 (1.847)		1.800 (1.801)
Pd–X' (Pd'–X')	2.363(5)	2.228 (2.350)	1.818 (1.810)	2.325 (2.332)
Bond angles (°)	6	II	II'	II''
Pd'–Pd–N	138.99(11)	126.5	160.8	138.6
Pd'–Pd–P	57.14(4)	53.8	56.1	56.3
N–Pd–P	82.62(12)	72.7	105.1	82.3
Pd'–Pd–P'	51.11(3)	53.3	70.0	56.5
N–Pd–P'	166.46(12)	164.2	144.9	167.2
P–Pd–P'	108.25(4)	107.1	110.1	112.8
P'–Pd–X'	44.83(13)	38.7	50.8	44.5
Pd–P–Pd'	71.75(4)	72.8	69.9	71.9
Pd'–P–X	65.80(17)	69.4	121.2	64.9
Pd'–X–P	69.37(17)	71.9	85.5	70.6

^a X = H₁ (**II** and **II'**), C_{ipso} of P(Ph) (**II''**), C₂₃ (**6**); X' = H₁' (**II** and **II'**), C'_{ipso} of P'(Ph') (**II''**), C₂₃' (**6**).

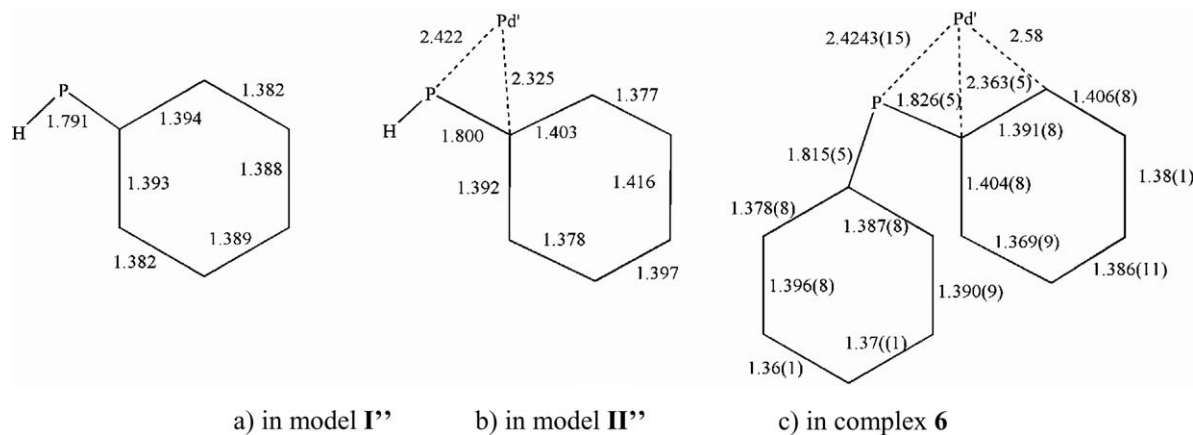


Fig. 5. Calculated bond distances within the phenyl rings in model compounds **II''** and **II'''**, and corresponding experimental values (X-ray data) of **6**.

tals. There are marked differences in the molecular energy schemes, notably the HOMO is of higher energy in **II''** than in **II** or **II'**. For all three model-species, the highest five occupied molecular orbitals all have high metal-character (localised mainly at the Pd–P–Pd'–P' ring) (Fig. 7(a)–(c)). Surprisingly, the most stabilised frontier orbitals show significant contributions of the H (in **II** or **II'**) or of the C_{ipso} (**II''**) of the bridging phosphines to the bonding interaction. Previously, theoretical predictions using ab initio calculations have been used to account for the bonding in compound [(dppp)Pd]₂(SO₃CF₃)₂ [27]. These ab initio calculations were performed only on [Pd(PH₃)₂]₂²⁺. It has been shown that for [Pd(PH₃)₂]₂²⁺, the tilting of the perpendicular Pd–P bonds toward the neighboring Pd atom creates an overlap between ‘unused’ Pd d_{xy} lobes and the lone pair of one of the phosphines that is already involved in dative bonding with the adjacent Pd atom. This makes the ‘side-on’ Pd–P interaction only weakly bonding. This

was believed to be the only means by which the unsaturated Pd atoms could relieve their coordinative unsaturation without losing the stabilisation of the dative bonds. This explanation was also found valid, at the DFT level, for the formation of the semi-bridging ‘side-on’ coordination of two phosphines in our models. However, the ab initio calculations on the [Pd(PH₃)₂]₂²⁺ model showed that the semi-bridging (or ‘side-on’) coordination of the P–PH₃ units to two Pd centres is obtained in the absence of a supporting Pd–(π-system) interaction [27]. Our DFT calculations demonstrate that the presence of aromatic substituents at the ligand should not be ignored for a more accurate model. The MO α 48 of [Pd₂{H(Ph)PCH₂CH=NH}₂]₂²⁺ (**II''**), shown in Fig. 7(c) supports the hypothesis of a delocalised interaction comprising the two Pd centres, the bridging phosphines and one phenyl group of the bridging phosphine in **II'**. In simplified models, where all the aromatic rings are replaced by hydrogen

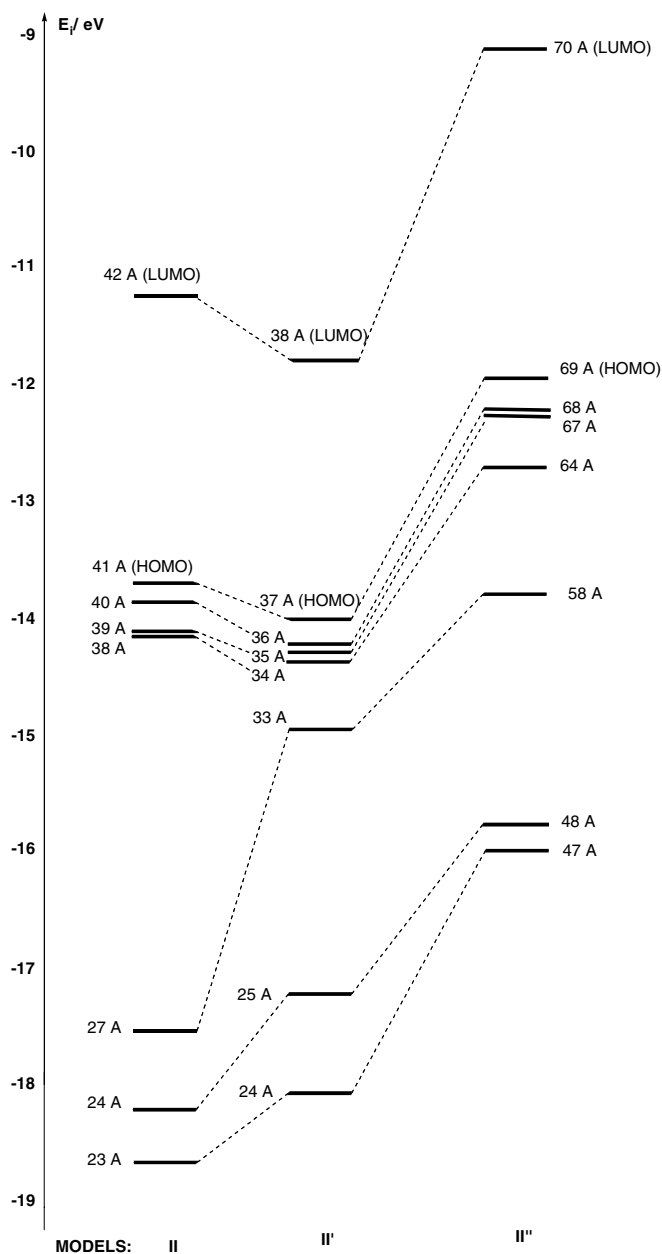


Fig. 6. MO schemes for **II**, **II'** and **II''**.

atoms (i.e. $[\text{Pd}_2(\text{H}_2\text{PCH}_2\text{CH}=\text{NH})_2]^{2+}$ (**II**) and $[\text{Pd}_2(\text{H}_3\text{P})_2(\text{NH}=\text{CH})_2]^{2+}$ (**II'**)) an extended Pd–P–H interaction occurs instead of this Pd–P– C_{ipso} interaction). This is illustrated for **II** by the molecular orbital α 27, shown in Fig. 7(a).

The atom–atom overlap population matrix showed that the palladium–palladium overlap is non-bonding in **II**, **II'** and **II''**. Significant bonding overlap was found between the atoms P and Pd' as well as between P' and Pd, for **II**, **II'** and **II''**, consistent with a semi-bridging phosphine group. In **II'**, the overlaps between C_{ipso} and Pd' and C_{ortho} (**1**) and Pd' (and similarly, between $C_{\text{ipso}'}$ and Pd, and $C_{\text{ortho}'}$ (**1**) and Pd) are only weakly bonding. In **II** and **II'** the over-

laps between atoms H₁ and Pd' and atoms H'₁ and Pd are also only weakly bonding.

It seems that the delocalised metal-phosphine–phenyl interaction plays an essential role in stabilising complexes of type $[\text{Pd}\{\text{Ph}_2\text{PCH}_2\text{C}(\text{Ph})=\text{N}(2,6\text{-R}_2\text{C}_6\text{H}_3)\}_2][\text{BF}_4]_2$, formally coordinatively unsaturated Pd(I) dimers which are remarkably inert with respect to air, moisture and electrophiles such as CO and ethylene. It is expected that the presence of bulky substituents at the imine centre in $[\text{Pd}\{\text{Ph}_2\text{PCH}_2\text{C}(\text{Ph})=\text{N}(2,6\text{-R}_2\text{C}_6\text{H}_3)\}_2][\text{BF}_4]_2$, R = *i*Pr (**5**) and Me (**6**) further enhances the kinetic stability of these complex by sheltering the metal centre as shown (for **6**) in Fig. 3(b).

3. Catalysis tests

3.1. CO–ethylene copolymerisation tests

We have previously shown that cationic species such as $[\text{PdMe}\{\text{Ph}_2\text{PCH}_2\text{C}(\text{Ph})=\text{N}(2,6\text{-Me}_2\text{C}_6\text{H}_3)\}]^+$ catalyse CO/ethylene copolymerisation when reactions are performed in CH_2Cl_2 under relatively mild conditions [34,35]. Here, the compounds $[\text{PdBr}_2\{\text{Ph}_2\text{PCH}_2\text{C}(\text{Ph})=\text{N}(2,6\text{-}^i\text{Pr}_2\text{C}_6\text{H}_3)\}]$ (**1**), $[\text{PdBr}_2\{\text{Ph}_2\text{PCH}_2\text{C}(\text{Ph})=\text{N}(2,6\text{-Me}_2\text{C}_6\text{H}_3)\}]$ (**2**), $[\text{Pd}_2(\mu\text{-Br})_2\{\text{Ph}_2\text{PCH}=\text{C}(\text{Ph})\text{N}(2,6\text{-}^i\text{Pr}_2\text{C}_6\text{H}_3)\}_2]$ (**3**) and $[\text{Pd}_2(\mu\text{-Br})_2\{\text{Ph}_2\text{PCH}=\text{C}(\text{Ph})\text{N}(2,6\text{-Me}_2\text{C}_6\text{H}_3)\}_2]$ (**4**) were also tested for their ability to catalyse the copolymerisation of CO and ethylene. CH_2Cl_2 solutions of the compounds were stirred for 2 h at room temperature, in the presence of 10 bar 1:1 CO:ethylene. A suspension of AgBF_4 and MeOH was also added, the presence of which was found by Drent et al. [38] to be necessary for the initiation step of the CO/ethylene copolymerisation catalysis of $[\text{Pd}(\text{dppp})][\text{SO}_3\text{CF}_3]_2$. No significant reduction of the autoclave pressure was observed during any of the polymerisation tests performed. In each case a black precipitate was formed whose infrared spectra did not contain a carbonyl stretch characteristic of poly($\text{C}_2\text{H}_4\text{-alt-CO}$) at 1692 cm^{-1} , and was shown by elemental analysis to be palladium black. This was assigned to the slow migratory insertion ensured by the trans influence of N/P ligand making the decomposition pathways relatively fast.

¹H NMR spectroscopy of the supernatants showed no trace of the pre-catalyst compounds. When complexes **3** and **4** were tested a small amount of orange crystals could be isolated from the liquid layer in each case after filtration, concentration under reduced pressure, layering with pentane and standing for 1 week at $-20\text{ }^\circ\text{C}$). Although NMR spectra proved to be broad and difficult to assign, these species were identified as the dications, $[\text{Pd}\{\text{Ph}_2\text{PCH}_2\text{C}(\text{Ph})=\text{N}(2,6\text{-R}_2\text{C}_6\text{H}_3)\}_2]^{2+}$, where R = *i*Pr (**5**) and Me (**6**), based on FAB⁺ and EI⁺ mass spectrometry. For R = Me, crystals obtained proved to be suitable for X-ray determination, which confirmed the molecular structure of **6**. An explanation for the inability of complexes $[\text{PdBr}_2(\text{HL1})]$ (**1**), $[\text{PdBr}_2(\text{HL2})]$ (**2**), $[\text{Pd}_2(\mu\text{-Br})_2(\text{L1})_2]$ (**3**) and $[\text{Pd}_2(\mu\text{-Br})_2(\text{L2})_2]$ (**4**) (where **HL1** = $[\text{Ph}_2\text{PCH}_2\text{C}(\text{Ph})=\text{N}(2,6\text{-R}_2\text{C}_6\text{H}_3)]$)

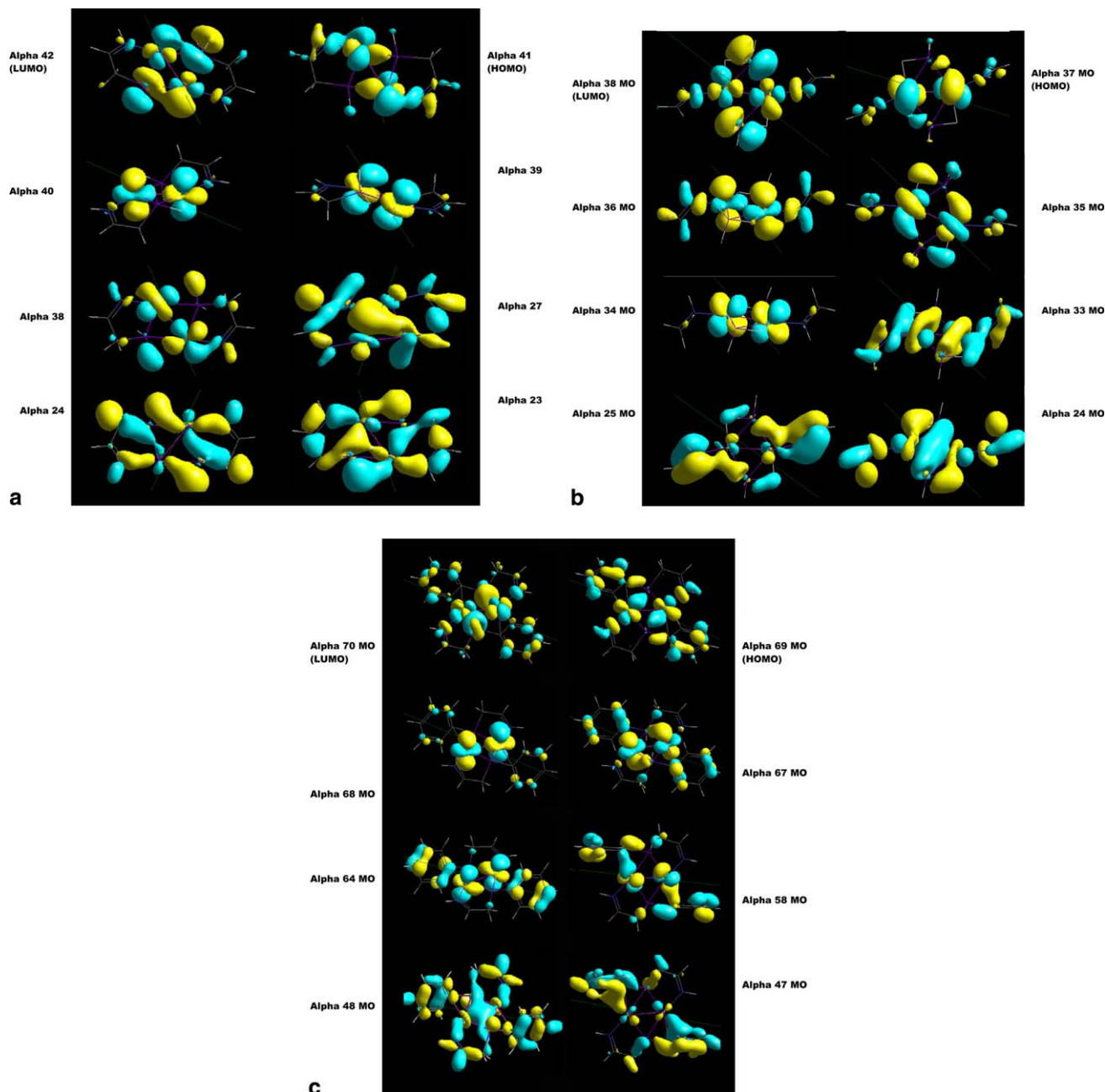


Fig. 7. Significant frontier molecular orbitals of the model complex **II** (a), **II'** (b) and **II** (c).

$N(2,6\text{-}i\text{Pr}_2\text{C}_6\text{H}_3)]$, $\text{L1}^- = [\text{Ph}_2\text{PCH}=\text{C}(\text{Ph})\text{N}(2,6\text{-}i\text{Pr}_2\text{C}_6\text{H}_3)]^-$, $\text{HL2} = [\text{Ph}_2\text{PCH}_2\text{C}(\text{Ph})=\text{N}(2,6\text{-Me}_2\text{C}_6\text{H}_3)]$, $\text{L2}^- = [\text{Ph}_2\text{PCH}=\text{C}(\text{Ph})\text{N}(2,6\text{-Me}_2\text{C}_6\text{H}_3)]^-$ to copolymerise CO and ethylene under the mild conditions above could be assigned to the rapid formation of kinetically stable Pd(I) dimers $[\text{Pd}\{\text{Ph}_2\text{PCH}_2\text{C}(\text{Ph})=\text{N}(2,6\text{-R}_2\text{C}_6\text{H}_3)\}]_2[\text{BF}_4]_2$, where $\text{R} = i\text{Pr}$ (**5**) and Me (**6**).

4. Conclusions

Novel Pd(II) and Pd(I) dimers have been synthesised and studied. These have been characterised spectroscopically and structures confirmed by X-ray diffraction. An insight into bonding within the new Pd(I) dimers with an unusual

geometry has been obtained by density functional theoretical investigations. For Pd(II)–halide complexes of bulky enolisable ligands such as $[\text{Ph}_2\text{PCH}_2\text{C}(\text{Ph})=\text{N}(2,6\text{-R}_2\text{C}_6\text{H}_3)]$, $\text{R} = \text{Me}$, $i\text{Pr}$, formation of Pd(I) dimers with remarkable stability towards electrophilic attack could hamper the alternating CO/ethylene copolymerisation process.

5. Experimental

5.1. General

All manipulations of air and/or moisture sensitive materials were performed under an inert atmosphere of pure Ar or dry N_2 using standard Schlenk line techniques or in an

inert atmosphere dry box. Inert gases were purified firstly by passage through columns filled with activated molecular sieves (4 Å) and then either manganese (II) oxide suspended on vermiculite, for the Schlenk line, or BASF catalyst, for the dry box. Celite filtration aid was purchased from Fluka Chemie and oven-dried at 150 °C prior to use. Solvents were pre-dried over activated 4 Å molecular sieves and then distilled under N₂ from Na/K alloy (light petroleum ether b.p. 40–60 °C, diethyl ether, pentane), from sodium (toluene), from potassium (THF), or from calcium hydride (dichloromethane). Deuterated NMR solvents (Aldrich, Goss Scientific) were refluxed and distilled from potassium metal (*d*⁸-toluene) or stirred overnight with calcium hydride (CD₂Cl₂) prior to use. Microanalyses were performed by the microanalytical laboratory of the Inorganic Chemistry Laboratory, University of Oxford and FAB⁺ mass-spectra by the EPSRC National Mass Spectrometry Service Centre, University of Wales, Swansea, UK.

NMR spectra were recorded using either a Varian Mercury-vx 300 (¹H 300 MHz, ¹³C 75.5 MHz, ¹⁹F 282.3 MHz, ³¹P 121.6 MHz) or a Varian UNITY plus (¹H 500 MHz, ¹¹B 160.4 MHz, ¹³C 125.7 MHz, ³¹P 202.4 MHz) spectrometer and are at room temperature unless otherwise stated. The spectra were referenced internally relative to the residual protio-solvent (¹H) and solvent (¹³C) resonances relative to tetramethylsilane (¹H, ¹³C, δ = 0) or externally to BF₃·Et₂O (¹¹B, δ = 0); H₃PO₄ (³¹P, δ = 0) or CFCl₃ (¹⁹F, δ = 0). Chemical shifts (δ) are expressed in ppm and coupling constants (*J*) in Hz.

GC–MS chromatographs and spectra were recorded using a Hewlett-Packard 5890 Gas Chromatograph fitted with a non-polar column connected to a Trio-1000 Mass Spectrometer operating Electron Impact (70 eV) and chemical ionisation (CI) mode (NH₃) and detecting positively charged species. The temperature profile for the GC is: 100 °C (3 min), then 10 °C/min ramp until 280 °C (held for 10 min).

Complexes [PdBr₂{Ph₂PCH₂C(Ph)=N(2,6-*i*-Pr₂C₆H₃)}] (**1**), [PdBr₂{Ph₂PCH₂C(Ph)=N(2,6-Me₂C₆H₃)}] (**2**) and [Pd₂(μ-Br)₂{Ph₂PCH=C(Ph)N(2,6-Me₂C₆H₃)}₂] (**4**) have been prepared following established procedures [34,35]. All new compounds were characterised by elemental analysis, FAB mass spectrometry, ¹H, ³¹P (and where applicable ¹⁹F and ¹¹B^δ NMR spectroscopy). In the case of **3**, **4b** (the second polymorph of **4**) and **6** the X-ray diffraction structures were determined.

5.1.1. Reaction between

[PdBr₂{Ph₂PCH₂C(Ph)=N(2,6-*i*-Pr₂C₆H₃)}] (**1**) and KH

[PdBr₂{Ph₂PCH₂C(Ph)=N(2,6-*i*-Pr₂C₆H₃)}] (**1**) (0.11 g, 0.15 mmol) and KH (0.006 g, 0.15 mmol) were mixed in a Schlenk tube and 50 mL cold THF was added whilst stirring at –78 °C. The reaction mixture was left stirring to reach room temperature over 12 h. The volatiles were removed under reduced pressure and the residue washed with 100 mL of pentane which gave a dark grey solid. The solid was extracted with 50 mL CH₂Cl₂ which gave

a purple solution. Removal of the volatiles under reduced pressure gave [Pd₂(μ-Br)₂{Ph₂PCH=C(Ph)N(2,6-*i*-Pr₂C₆H₃)}₂] (**3**) as a green solid.

*Spectroscopic data for [Pd₂(μ-Br)₂{Ph₂PCH=C(Ph)N(2,6-*i*-Pr₂C₆H₃)}₂] (**3**).* Elemental analysis Calc.: C, 59.23; H, 5.13; N, 2.16. Found: C, 58.6; H, 5.3; N, 2.05%. Mass spectrum (FAB⁺) *m/z* 1307.93(100) [M + H]⁺.

¹H NMR (500 MHz, CD₂Cl₂): 1.45 (d, CH₃CHCH₃, 12H, ³*J*_{HH} = 6.8), δ = (d, CH₃CHCH₃, 12H, ³*J*_{HH} = 6.8), 3.43 (h, CH₃CHCH₃, 4H, ³*J*_{HH} = 6.8), 3.49 (d, *CHP*, 2H, ³*J*_{PH} = 8.5 Hz), 6.80 (d, 4 H, *m*-H of 2,6-*i*-Pr₂C₆H₃), 7.03 (t, 2H, *p*-H of 2,6-*i*-Pr₂C₆H₃), 7.05 (m, 4H, *m*-H of *Ph*-C), 7.18 (m, 2H, *p*-H of *Ph*-C), 7.23 (m, 4H, *o*-H of *Ph*-C), 7.44 (m, 8H, *m*-H of *PPh*₂), 7.52 (m, 4H, *p*-H of *PPh*₂), 7.75 (m, 8H, *o*-H of *PPh*₂).

¹³C{¹H} NMR (125.7 MHz, CD₂Cl₂): 23.6 (s, CH₃CHCH₃), 24.8 (s, CH₃CHCH₃), 28.5 (s, CH₃CHCH₃), 72.1 (d, *CH*-P, ¹*J*_{PC} = 65 Hz), 177.6 (d, N=C, ²*J*_{PC} = 23), 145.2 (s, *i*-C of ⁱPr₂C₆H₃N), 139.7 (s, *o*-C of ⁱPr₂C₆H₃N), 127.1 (s, *m*-C of ⁱPr₂C₆H₃N), 123.1 (s, *p*-C of ⁱPr₂C₆H₃N), 132.9 (b, *i*-C of *Ph*), 130.9 (s, *o*-C of *Ph*), 128.6 (s, *m*-C of *Ph*), 128.4 (s, *p*-C of *Ph*), 132.5 (d, *o*-C of *PPh*₂, ²*J*_{PC} = 11), 129.5 (d, *m*-C of *PPh*₂, ³*J*_{PC} = 12), 133.2 (d, *p*-C of *PPh*₂, ²*J*_{PC} = 11).

³¹P{¹H} NMR (202.4 MHz, CD₂Cl₂): 53.8 (s).

5.1.2. Reaction between [Pd₂(μ-Br)₂{Ph₂PCH=C(Ph)-N(2,6-Me₂C₆H₃)}₂] (**4**), AgBF₄ and MeOH

The solids [Pd₂(μ-Br)₂{Ph₂PCH=C(Ph)N(2,6-Me₂C₆H₃)}₂] (**4**) (0.015 g, 0.0127 mmol) and AgBF₄ (0.007 g, 0.0253 mmol) were mixed in a Schlenk tube and a mixture of 25 mL CH₂Cl₂ and 1 mL MeOH was added via cannulae. The reaction mixture was stirred for 1 h at room temperature which gave a black residue and a yellow supernatant. The black residue formed was removed by filtration. The yellow supernatant was concentrated under reduced pressure to about 5 mL and layered with pentane. After storing for 2 days at 0 °C, yellow-orange crystals were isolated from the mixture and characterised as [Pd{Ph₂PCH₂C(Ph)=N(2,6-Me₂C₆H₃)}₂][BF₄]₂ (**6**). Yield 30%.

*Spectroscopic data for [Pd₂{Ph₂PCH₂C(Ph)=N(2,6-Me₂C₆H₃)}₂][BF₄]₂ (**6**).* Elemental analysis Calc.: C, 56.0; H, 4.4; N, 2.3. Found: C, 55.4; H, 4.32; N, 1.92%. Mass spectrum (FAB⁺) *m/z* 1026.6 (45) [M – 2BF₄]²⁺, IR (CD₂Cl₂)_νC=N 1538 cm⁻¹, _νBF₄ 1400 cm⁻¹.

¹H NMR data (500 MHz, CD₂Cl₂) 2.30 (s, 12H, Me₂C₆H₃), 5.17 (d, 4H, *CH*₂-P, ²*J*_{PH} = 13.4), 6.90 (b, 2H, *p*-H of Me₂C₆H₃), 6.86 (d, 4H, *m*-H of Me₂C₆H₃, ³*J*_{HH} = 7.6), 7.25 (m, 4H, *o*-H of *Ph*), 7.10 (m, 4H, *m*-H of *Ph*), 7.32 (m, 2H, *p*-H of *Ph*), 7.61 (m, 4H, *o*-H of *PPh*₂, ³*J*_{PH} = 13.4), 7.46 (m, 4H, *m*-H of *PPh*₂, ⁴*J*_{PH} = 2.7), ³¹P{¹H} NMR data (202.4 MHz, CD₂Cl₂) 47.9 (s), ¹¹B{¹H} NMR data (160.4 MHz, CD₂Cl₂) –0.2 (s), ¹⁹F NMR data (282.45 MHz, CD₂Cl₂) –150.0 (s), ¹³C{¹H} NMR data (125.7 MHz, CD₂Cl₂): 19.0 (s, Me₂C₆H₃N), 68.4 (b, *CH*₂-P), 133–125 (12 aromatic-C resonances).

The identical procedure was followed for the reaction between $[\text{Pd}_2(\mu\text{-Br})_2\{\text{Ph}_2\text{PCH}=\text{C}(\text{Ph})\text{N}(2,6\text{-}^i\text{Pr}_2\text{C}_6\text{H}_3)\}_2]$ (**3**) (0.015 g, 0.0116 mmol), AgBF_4 (0.007 g, 0.0253 mmol) and MeOH (1 mL). Complex $[\text{Pd}\{\text{Ph}_2\text{PCH}_2\text{C}(\text{Ph})=\text{N}(2,6\text{-}^i\text{Pr}_2\text{C}_6\text{H}_3)\}_2][\text{BF}_4]_2$ (**5**) was isolated as a microcrystalline orange powder with less than 15% yield.

Spectroscopic data for $[\text{Pd}_2\{\text{Ph}_2\text{PCH}_2\text{C}(\text{Ph})=\text{N}(2,6\text{-}^i\text{Pr}_2\text{C}_6\text{H}_3)\}_2][\text{BF}_4]_2$ (**5**).

Mass spectrum: $(\text{EI}^-) m/z$ 87.66 (100) $[\text{BF}_4]^+$; $(\text{FAB}^+) m/z$ 1024.06(45) $[\text{M} - 2\text{BF}_4]$, 488.97(100) $[1/2(\text{M} - 2\text{Ph} - 2\text{BF}_4)]$, IR (CD_2Cl_2) $\nu_{\text{C}=\text{N}}$ 1538 cm^{-1} , ν_{BF_4} 1400 cm^{-1} .

^1H NMR (500 MHz, CD_2Cl_2): 0.18 (d, CH_3CHCH_3 , 6H, $^3J_{\text{HH}} = 6.5$), 0.87 (d, CH_3CHCH_3 , 6H, $^3J_{\text{HH}} = 7$), 0.50 (d, CH_3CHCH_3 , 6H, $^3J_{\text{HH}} = 6.5$), 1.41 (d, CH_3CHCH_3 , 6H, $^3J_{\text{HH}} = 7$), 2.80 (h, CH_3CHCH_3 , 2H, $^3J_{\text{HH}} = 6.5$), 3.20 (h, CH_3CHCH_3 , 2H, $^3J_{\text{HH}} = 7$), 5.04 (broad d, $\text{CH}_2\text{-P}$, 4H, $^3J_{\text{PH}} = 14.1$ Hz), 7.21 (d, *m*-H of 2,6- $^i\text{Pr}_2\text{C}_6\text{H}_3$, 4H $^3J_{\text{HH}} = 7.5$), 7.25 (b, *p*-H of 2,6- $^i\text{Pr}_2\text{C}_6\text{H}_3$, 2H), 7.03–7.31 (multiple aromatic resonances, 20H), 8.08 (m, 4H, *m*-H of *PPh*), 7.98 (m, 2H, *p*-H of *PPh*), 8.20 (m, 4H, *o*-H of *PPh*). $^{31}\text{P}\{^1\text{H}\}$ NMR data (202.4 MHz, CD_2Cl_2) 50.4 (s), $^{11}\text{B}\{^1\text{H}\}$ NMR data (160.4 MHz, CD_2Cl_2) –0.375 (s), ^{19}F NMR data (282.45 MHz, CD_2Cl_2) –132.8 (s).

5.2. Copolymerisation tests

The catalyst (0.044 mmol) was treated with AgBF_4 (0.02 g, 0.088 mmol) and 10 mL MeOH in 200 mL CH_2Cl_2 in a Schlenk tube. After 30 min stirring at room temperature, this mixture was transferred into a dried 1 L Parr autoclave and equipped with a stirrer bar. The autoclave was charged with 10 bar 1:1 C_2H_4 :CO mixture, and maintained at the room temperature for 2 h. No significant

reduction of the autoclave pressure was observed during any of the polymerisation tests. Subsequently, the remaining C_2H_4 /CO gas mixture was vented. A sample from the solution was collected for GC–MS. The copolymerisation was quenched with MeOH and HCl. No formation of copolymer was observed. In each case a black precipitate was formed whose infrared spectra did not contain a carbonyl stretch characteristic of poly(C_2H_4 -alt-CO) at 1692 cm^{-1} , and was shown by elemental analysis to be palladium black. Although ^1H NMR spectroscopy of the supernatants showed no trace of the pre-catalysts **1** (or **2**) a series of unidentifiable ligand-containing species was present in the mixture. GC–MS analysis of the liquid layer indicated no formation of oligomers.

5.3. X-ray crystallography

In each case, a single crystal was selected under an inert atmosphere, encased in perfluoro-polyether oil, and mounted on the end of a glass fibre. The fibre, secured in a goniometer head was then placed under a stream of cold nitrogen maintained at 150 K and data collected on an Enraf-Nonius DIP2000 image plate diffractometer with graphite monochromated Mo $\text{K}\alpha$ radiation ($\lambda = 0.71069$ Å) The images were processed with the DENZO and SCALEPACK programs [40–42] and corrections for Lorentz and polarisation effects were performed.

The structures of **3b**, **4** and **6** were solved by direct methods using the SIR92 program [43] and refined by full-matrix least-squares procedure on *F*. All solution, refinement, and graphical calculations were performed using the CRYSTALS [44] and CAMERON [45] software packages. The crystallographic data are summarised in Table 3. In each case, all

Table 3
Selected crystallographic data for studied complexes

Compound	3	4b	6
Formula	$\text{C}_{64}\text{H}_{66}\text{Br}_2\text{N}_2\text{P}_2\text{Pd}_2$, CH_2Cl_2	$\text{C}_{56}\text{H}_{50}\text{Br}_2\text{N}_2\text{P}_2\text{Pd}_2$	$\text{C}_{56}\text{H}_{52}\text{N}_2\text{P}_2\text{Pd}_2$, $2(\text{BF}_4)$
<i>M</i>	1382.69	1185.56	1201.40
<i>T</i> /K	150(2)	150(2)	150(2)
Crystal system	triclinic	triclinic	orthorhombic
Space group	$P\bar{1}$	$P\bar{1}$	<i>Pcab</i>
<i>a</i> /Å	9.3069(2)	8.9087(2)	14.8791(4)
<i>b</i> /Å	13.7945(3)	11.1979(3)	16.7617(5)
<i>c</i> /Å	24.3989(5)	13.7910(5)	20.3280(7)
α /°	82.8645(8)	71.6166(13)	90
β /°	89.1140(9)	79.8146(13)	90
γ /°	76.5895(12)	66.578(2)	90
<i>V</i> /Å ³	3023.13(11)	1195.89(6)	5069.8(3)
<i>Z</i>	2	1	4
$\rho_{\text{calc}}/\text{g cm}^{-3}$	1.519	1.646	1.574
μ/mm^{-1}	2.099	2.530	0.843
$\theta_{\text{max}}/\text{°}$	27.48	27.62	27.47
Total data	13853	5557	5806
Unique data	6533	3014	3101
<i>R</i> _{int}	0.05	0.04	0.04
<i>R</i> [<i>I</i> > 3σ(<i>I</i>)]	0.0512	0.0466	0.0451
<i>wR</i>	0.1113	0.0601	0.0367
Goodness-of-fit	1.1098	1.1346	0.0878
ρ minimum and ρ maximum	–1.84 and 2.12	–0.93 and 1.15	–0.88 and 0.87

non-hydrogen atoms were refined with anisotropic displacement parameters and hydrogen atoms were generated and allowed to ride on their corresponding carbon atoms with fixed thermal parameters. Empirical absorption correction were applied, as well as the three-term Chebyshev polynomial weighting scheme [46].

The crystal structures have been deposited at the Cambridge Crystallographic Data Centre, CCDC Nos. 288353–288355.

5.4. Computational details

ADF [47] calculations were performed using Vosko, Wilke and Nusair's local functional [48] with the Becke 88 [49] and the Perdew 86 [50] non-local exchange and correlation gradient corrections, on ADF version 2000.02 [49,51–53]. The basis sets used were uncontracted triple-n Slater-type orbitals (STOs). The cores of the atoms were frozen up to 3d for Pd, 1s for C and N, 2p for P.

Acknowledgements

We thank the Royal Society for a University Research Fellowship (SIP) and EPSRC for financial support.

References

- [1] U. Christmann, R. Vilar, *Angew. Chem. Int. Ed.* 44 (2005) 366.
- [2] V. Dura-Vila, D.M.P. Mingos, R. Vilar, A.J.P. White, D.J. Williams, *Chem. Commun.* (2000) 1525.
- [3] U. Nettekoven, F. Naud, A. Schnyder, H.U. Blaser, *Synlett* (2004) 2549.
- [4] U. Christmann, R. Vilar, A.J.P. White, D.J. Williams, *Chem. Commun.* (2004) 1294.
- [5] T. Murahashi, H. Kurosawa, *Coord. Chem. Rev.* 231 (2002) 207.
- [6] M. Jorgensen, S. Lee, X.X. Liu, J.P. Wolkowski, J.F. Hartwig, *J. Am. Chem. Soc.* 124 (2002) 12557.
- [7] D. Zim, S.L. Buchwald, *Org. Lett.* 5 (2003) 2413.
- [8] J. Vicente, J.A. Abad, E. Martinez-Viviente, P.G. Jones, *Organometallics* 22 (2003) 1967.
- [9] J. Vicente, J.A. Abad, E. Martinez-Viviente, P.G. Jones, *Organometallics* 21 (2002) 4454.
- [10] G. Allegra, G.T. Casagrande, A. Immirzi, L. Porri, G. Vitulli, *J. Am. Chem. Soc.* 92 (1970) 289.
- [11] B. Calmuschi, U. Englert, *Acta Crystallogr., Sect. C* 58 (2002) M545.
- [12] T. Murahashi, T. Otani, T. Okuno, H. Kurosawa, *Angew. Chem., Int. Ed.* 39 (2000) 537.
- [13] P. Espinet, J. Fornies, C. Fortuno, G. Hidalgo, F. Martinez, M. Tomas, A.J. Welch, *J. Organomet. Chem.* 317 (1986) 105.
- [14] P. Dotta, P.G.A. Kumar, P.S. Pregosin, A. Albinati, S. Rizzato, *Organometallics* 23 (2004) 4247.
- [15] Y. Tatsumi, T. Naga, H. Nakashima, T. Murahashi, H. Kurosawa, *Chem. Commun.* (2004) 1430.
- [16] G. Nardin, P. Delise, G. Allegra, *Gazz. Chim. Ital.* 105 (1975) 1047.
- [17] M. Gorlov, A. Fischer, L. Kloo, *Inorg. Chim. Acta* 350 (2003) 449.
- [18] M. Gorlov, A. Fischer, L. Kloo, *J. Organomet. Chem.* 689 (2004) 489.
- [19] M. Sommovigo, M. Pasquali, P. Leoni, D. Braga, P. Sabatino, *Chem. Ber.* 124 (1991) 97.
- [20] C.C. Lu, J.C. Peters, *J. Am. Chem. Soc.* 124 (2002) 5272.
- [21] A.J. Davenport, D.L. Davies, J. Fawcett, D.R. Russell, *J. Chem. Soc., Dalton Trans.* (2002) 3260.
- [22] G. Garcia-Herbosa, A. Munoz, D. Miguel, S. Garcia-Granda, *Organometallics* 13 (1994) 1775.
- [23] C. Navarro-Ranninger, F. Zamora, L.A. Martinez-Cruz, R. Isea, J.R. Masaguer, *J. Organomet. Chem.* 518 (1996) 29.
- [24] J.W. Suggs, M.J. Dube, M. Nichols, *Chem. Commun.* (1993) 307.
- [25] M. Ghedini, D. Pucci, G.d. Munno, D. Viterbo, F. Neve, S. Armentano, *Chem. Mater.* 3 (1991) 65.
- [26] A.C. Albeniz, P. Espinet, B. Martin-Ruiz, *Chem. Eur. J.* 7 (2001) 2481.
- [27] P.H.M. Budzelaar, P.W.N.M.v. Leeuwen, C.F. Roobeek, *Organometallics* 11 (1992) 23.
- [28] M. Retboll, A.J. Edwards, A.D. Rae, A.C. Willis, M.A. Bennett, E. Wenger, *J. Am. Chem. Soc.* 124 (2002) 8348.
- [29] Y.-J. Kim, X. Chang, J.-T. Han, M.S. Lim, S.W. Lee, *Dalton Trans.* (2004) 3699.
- [30] B. Soro, S. Stoccoro, G. Minghetti, A. Zucca, M.A. Cinellu, S. Gladioli, M. Manassero, M. Sansoni, *Organometallics* 24 (2005) 53.
- [31] P. Braunstein, U. Englert, G.E. Herberich, M. Neuschütz, *Angew. Chem., Int. Ed.* 34 (1995) 1010.
- [32] N.G. Jones, M.L.H. Green, I.C. Vei, L.H. Rees, S.I. Pascu, D. Watkin, A. Cowley, X. Morise, P. Braunstein, *Dalton Trans.* (2002) 2491.
- [33] S.I. Pascu, K.S. Coleman, A.R. Cowley, M.L.H. Green, N.H. Rees, *J. Organomet. Chem.* 690 (2005) 1645.
- [34] S.I. Pascu, K.S. Coleman, A.R. Cowley, M.L.H. Green, N.H. Rees, *New J. Chem.* 29 (2005) 385.
- [35] K.S. Coleman, M.L.H. Green, S.I. Pascu, N.H. Rees, A.R. Cowley, L.H. Rees, *Dalton Trans.* (2001) 3384.
- [36] X. Liu, K.F. Mok, P.-H. Leung, *Organometallics* 20 (2001) 3918.
- [37] M.H.L. Green, *J. Organomet. Chem.* 500 (1995) 127.
- [38] E. Drent, P.H.M. Budzelaar, *Chem. Rev.* 96 (1996) 663.
- [39] W. Lin, S.R. Wilson, G.S. Girolami, *Inorg. Chem.* 33 (1994) 2265.
- [40] Z. Otwinowski, W. Minor, *Methods Enzymol.* (1996) 276.
- [41] Z. Otwinowski, W. Minor, *Methods Enzymol.* 26 (1997) 343.
- [42] Z. Otwinowski, W. Minor, *Methods Enzymol.* 276 (1997) 307.
- [43] A. Altomare, G. Carascano, C. Giacovazzo, A. Guagliardi, *J. Appl. Crystallogr.* 26 (1993) 343.
- [44] D.J. Watkin, C.K. Prout, J.R. Carruthers, P.W. Better, *CRYSTALS*, Oxford, 1996.
- [45] D.J. Watkin, C.K. Prout, L.J. Pearce, *CAMERON*, Oxford, 1996.
- [46] N. Walker, D. Stuart, *Acta Crystallogr., Sect. A* 39 (1983) 158.
- [47] B. te Velde, E.J. Baerends, *J. Comput. Phys.* 99 (1992) 84.
- [48] S.H. Vosko, L. Wilk, M. Nusair, *Can. J. Phys.* 58 (1990) 1200.
- [49] A.D. Becke, *Phys. Rev. A* 38 (1988) 2398.
- [50] J. Perdew, *Phys. Rev. B* 33 (1986) 8822.
- [51] L. Verluis, T. Ziegler, *J. Chem. Phys.* 88 (1988) 322.
- [52] C. Fonseca Guerra, J.G. Snijder, B. te Velde, E.J. Baerends, *Theor. Chem. Acc.* 99 (1998) 391.
- [53] E.J. Baerends, E.G. Ellis, P. Ros, *Chem. Phys.* 2 (1973) 41.